Recurrent Spatio-temporal Structures in Presence of Continuous Symmetries

Xiong Ding

September 3, 2015

Abstract

Invariant subsets inside a chaotic flow, such as equilibria, periodic orbits and invariant tori, play the key role in shaping the geometry of the global attractor (or inertial manifold). The goal of my research is to understand how chaotic attractor is organized by the set of (relative) periodic orbits and sort them by their weighted contributions to the spatio-temporal averages of observables measured on the attractor. In order to achieve this goal, technical advances on two directions need to be surmounted. First, the accuracy of stability analysis of (relative) periodic orbits is needed to be brought to a level much higher than the standard methods available in the literature, to establish whether the Floquet vectors evaluated along (relative) periodic orbits are a tool for estimating the local dimension of system's inertial manifold. Second, while it is already known that for systems with discrete and/or continuous symmetries, dynamics can be substantially simplified if symmetries are quotiented, one still needs to establish that the dynamical zeta functions and spectral determinants are decomposed into irreducible representations of the continuous symmetries of the flow. This thesis proposal introduces the background for conducting research in this area, summarizes the work I have done so far, and outlines the plan for my future work.

1 Introduction

1.1 Cycle averaging formulas

Statistical properties and geometrical structure are among the major questions in the study of chaotic nonlinear dissipative systems. Generally, such a system will get trapped to a invariant set, which is called global (maximal) attractor after a transient period, and we are only interested in the dynamics on the attractor, especially the temporal physical quantities such as average diffusion rate, energy dissipation rate, Lyapunov exponents and so on. The intrinsic instability of orbits on the attractor make the long time simulation unreliable, which is also time consuming. According to the ergodic theorem [17], long time averaging converges to the same answer as a spatial average over the attractor, provided we know the natural measure on the attractor. However, as a strange attractor usually has support on a fractal structure, and a non-continuous measure, such computations are not numerically feasible. This is where the periodic orbit theory [12] enters. Invariant subset accompanied with their stable/unstable manifolds shape the orbits on global attractor. Usually, we can find a few equilibria (or relative equilibria if system possesses continuous symmetries), and a dense, zero measure set of (relative) periodic orbits. Predecessors proved a direct link

between a weighted sum of physical quantities on periodic orbits and the long time averages in the form of *spectral determinant* [4]

$$\det(s-\mathcal{A}) = \exp\left(-\sum_p \sum_{r=1}^{\infty} \frac{1}{r} \frac{e^{r(\beta A_p - sT_p)}}{\left|\det\left(\mathbf{1}-M_p^r\right)\right|}\right), \tag{1}$$

where subscript p denote the periodic orbits, M_p is the monodromy matrix along a periodic orbit, A_p is the physical observable integrated along the orbit $A(x_0,t) = \int_0^t d\tau\, a(x(\tau))$ and T_p is the period. The largest zero point $s(\beta)$ of (1) is a implicit function of parameter β, and it is claimed that average of $a(x(t))$ is given by

$$\left.\frac{\partial s}{\partial \beta_j}\right|_{\beta=0} = \langle a_j \rangle \tag{2}$$

Note, the above sum involves the summation of all periodic orbits inside this system. In practice, we truncate (1) according to the topological length of periodic orbits, which is primarily established by symbolic dynamics, or if not available, by stability of periodic orbits. This technique is called *cycle expansion*, whose effectiveness has been demonstrated in a few 1-dimensional maps [2, 3] and ergodic flows [6, 8, 24].

1.2 Inertial manifold

Symbolic dynamics provides a complete topological description on the attractor. However, in practice, it is difficult to extract such simplified dynamics on strange attractor, especially for high dimensional turbulent flows. Also, other geometric properties are interesting but beyond the capability of symbolic dynamics. One such property is the effective dimension of attractor. For dissipative systems, global attractor is a measure-zero invariant subset of the state space concerned, and usually has non-smooth surface and fractal dimension, which make it hard to analyze, so we wish to use a 'tight' smooth manifold that encloses it but has nicer properties. This is called *inertial manifold* [19, 32]. These two concepts are different mainly by their local properties. Each point on inertial manifold with its neighborhood behaves as $\mathbb{R}^M$ (homeomorphic to an open subset of $\mathbb{R}^M$) with integer number M the dimension of inertial manifold. For a strange attractor, the scenario is much more complicated. Also, we need to explain the meaning of 'tight'. It refers to the fact that it is a forward invariant manifold with lowest dimension that encloses the global attractor and attracts points in the state space exponentially fast.

The existence of global attractor and/or inertial manifold has been proved for many chaotic or turbulent systems [32]. Also numerical methods such as Euler-Galerkin [18], nonlinear Galerkin method [26] to approximate inertial manifold have been proposed, but the discussion of all these methods focuses on the performance over standard Galerkin method. Little is known about the exact dimension of inertial manifold except a few systems [32]. For our interest in 1-dimensional Kuramoto-Sivashinsky equation, only upper bound, to the best knowledge of the author, is given as proportional to $L^{2.46}$ [22, 28], which is far above our linear relation expectation in spatiotemporal chaos.

On the other hand, the progress in numerical method to calculate *covariant vectors* [20, 23] motivated physicists to try to expand inertial manifold by covariant vectors locally through statistical study of the tangency among covariant vectors [34] and difference vector projection [33]. The number of the covariant vectors needed for a faithful expansion is

regarded as the dimension of inertial manifold. The key observation in this study is that tangent space can be decomposed of an entangled physical subspace and a contracting disentangled subspace, and the latter is thought to be irrelevant to the long time behavior on the inertial manifold. Similar properties have been observed on Floquet vectors associated with periodic orbits inside Kuramoto-Sivashinsky equation, so we expect to get the same result about the dimension of inertial manifold by focusing on periodic orbits instead of a long ergodic trajectory. Also, our work focuses on the continuous symmetry reduced space, whose inertial manifold is one dimension less than that in the original space.

1.3 Covariant algorithm and Periodic Schur Decomposition

Physicists are trying to understand dynamical systems by topological invariant objects inside these systems, such as equilibria, periodic orbits, invariant tori, etc. For instance, The *multiplicative ergodic theorem* (Oseledets theorem) [27, 30] states that there is an forward and backward invariant subspace $W_i(x)$ associated with each Lyapunov exponent λ_i in dynamical systems.

$$\lim_{t\to\pm\infty} \frac{1}{|t|} \ln \parallel J^t(x)u \parallel = \pm\lambda_i\,, \quad u \in W_i(x) \tag{3}$$

If a Lyapunov exponent has degeneracy one, the corresponding subspace $W_i(x)$ reduces to a vector, called *covariant vector*. This statement dates back to 1960's, but the corresponding numerical algorithms are invented quite recently, which is also the basis of the work on investigating the dimension of inertial manifold mentioned in sec. 1.2. Our Floquet vector algorithm in sec. 2.1 is motivated by covariant vector algorithm. Also, for periodic orbits, λ_i coincide with the real part of Floquet exponents, and subspace $W_i(x)$ coincides with a Floquet vector, or, if there is degeneracy, a subspace spanned by the degenerate Floquet vectors.

Another algorithm, Periodic Schur Decomposition [5], is also the basis of our Floquet vector algorithm. This algorithm enables us to calculate the eigenvalues of the product of a sequence of square matrices without forming the product it explicitly. This scenario happens in the stability analysis of periodic orbits in dynamical system since monodromy matrix follows the chain rule and thus can be decomposed as the product of a sequence of matrices. We should mention that Periodic Schur Decomposition transforms individual matrices into upper-triangular or quasi-upper triangular form, so eigenvalues are manifest as the product of diagonal elements of all these matrices; however, to obtain the corresponding eigenvectors or a subset of eigenvectors, we need to take further steps based on Periodic Schur Decomposition, which is illustrated in sec. 2.1.

1.4 Intermittent explosion in cubic quintic complex Ginzburg-Landau equation

Derived as a general amplitude equation near bifurcation point, complex Ginzburg-Landau equation [11] has ubiquitous applications in various areas of physics, and serves as a prototype for a lot of other equations such as nonlinear Schrödinger equation. Its cubic form is frequently used to study turbulence and intermittent traveling waves. But, recently, complex Ginzburg-Landau equation with a cubic quintic nonlinear term attracts much attention for its peculiar intermittent explosion of soliton solution in one dimensional and two

dimensional cases. Here, we focus on the one dimensional quintic complex Ginzburg-Landau equation defined on a periodic domain

$$A_t = \mu A + DA_{xx} + \beta|A|^2A + \gamma|A|^4A\,, \quad x \in [0, L]\,. \tag{4}$$

Here, $A(x,t)$ is a complex field. Coefficient μ is real and the other three coefficients are complex.

$$D = D_r + iD_i\,, \quad \beta = \beta_r + i\beta_i\,, \quad \gamma = \gamma_r + i\gamma_i\,.$$

Parameters are fixed to $D = 0.125 + 0.5i$, $\beta = 1 + 0.8i$, $\gamma = -0.1 - 0.6i$, $L = 50$.

Since β has positive real part, cubic quintic complex Ginzburg-Landau equation undergoes subcritical bifurcation at $\mu = 0$. Moreover, as shown in ref. [13], increasing μ from very negative to zero, the system undergoes stable pulses, oscillating pulses with one frequency, pulses with two frequency, and symmetric/asymmetric explosion. We set $\mu = -0.213$ the same as in refs. [14, 10, 9, 1] to observe symmetric and asymmetric explosion as shown in figure 1.

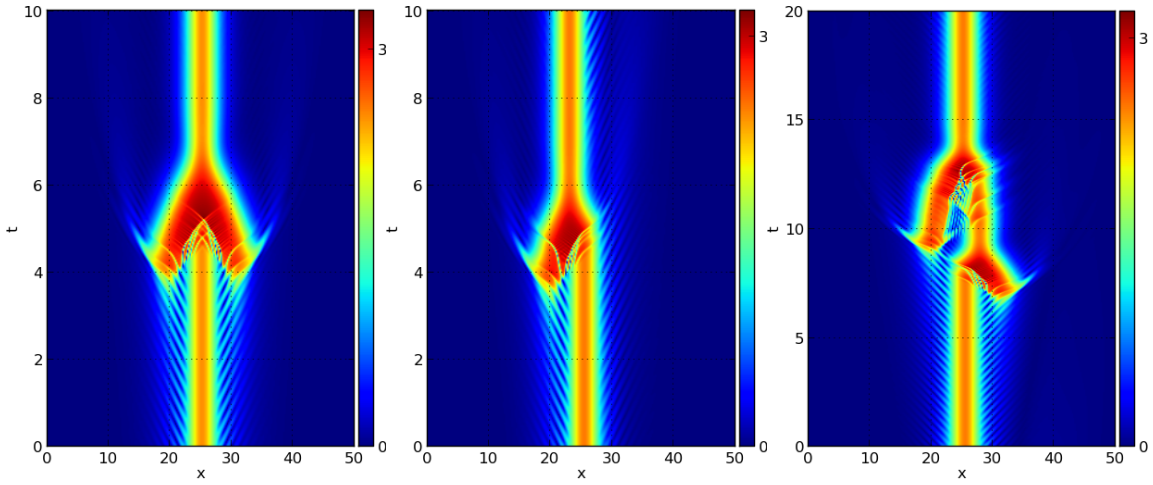

Figure 1: Three different types of soliton explosion: symmetric, asymmetric type 1, asymmetric type 2. $\mu = -0.1$. Color represents the magnitude of A.

At present, no precursor to the explosion has been found and it is unclear how the explosion frequency depends on the system size and parameters. Also, you can see that the center of mass of the localized soliton stays unchanged under symmetric explosion and shifts left or right under asymmetric explosion. Such a phenomenon is also observed in the 2-dimensional case [7]. So one of our goals of undertaking this system is to calculate the diffusion coefficient of the solition by cycle expansion. Recently, people [14, 10, 9, 1, 15, 7] use different approximation schemes to explain this phenomenon and and test their predictions by numerical experiments. However, little has been shed on the unstable invariant solutions in this system, nor their stability analysis.

On the other hand, Cubic quintic complex Ginzburg-Landau (4) has three symmetries:

- **translational symmetry**. $\tau_\ell A(x,t) = A(x+\ell, t)$.
- **phase invariance**. $\rho_\phi A(x,t) = e^{i\phi}A(x,t)$.
- **symmetric reflection**.$R_s A(x,t) = A(-x,t)$.

Previous research does not leverage the continuous/discrete symmetries of this system. We will simplify the state space by reducing the symmetries and then apply cycle expansion theory.

2 Preliminary results

2.1 Computing Floquet vectors by Periodic Eigendecomposition

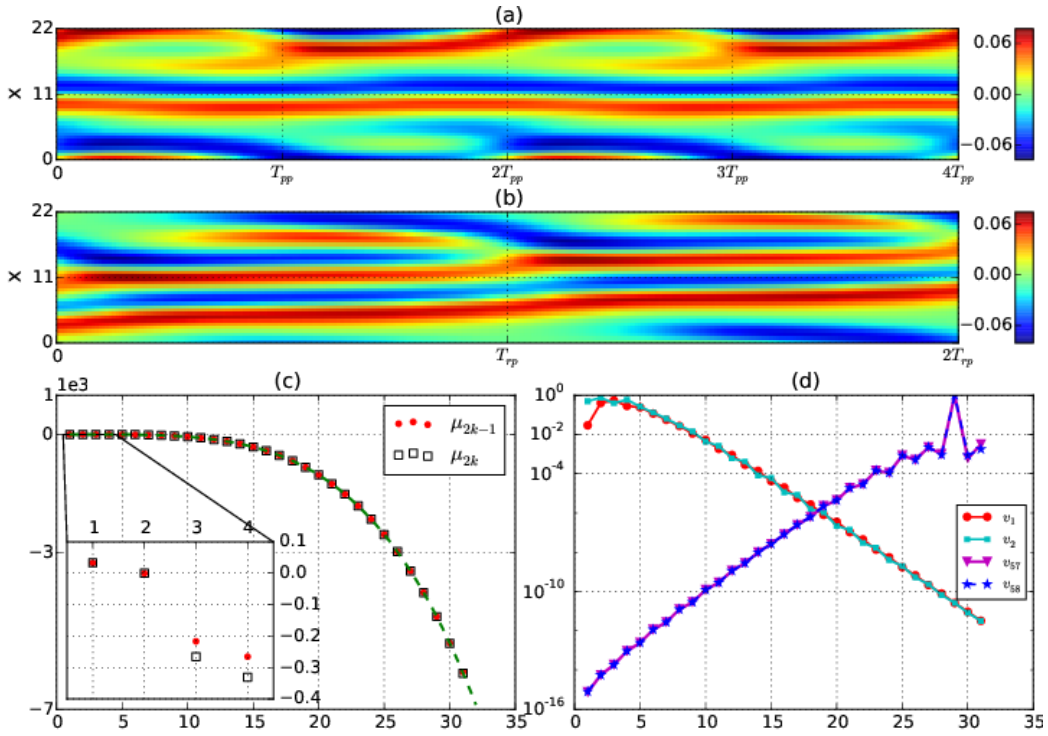

Figure 2: (Color online) (a) Preperiodic orbit $\overline{pp}_{10.25}$ and (b) relative periodic orbit $\overline{rp}_{16.31}$ in the full state space for total time $4\,T_{pp}$ and $2\,T_{rp}$, respectively. The phase shift for $\overline{rp}_{16.31}$ after one prime period $\simeq -2.863$. (c) The real parts of Floquet exponents paired for a given k as $(k, \mu^{(2k-1)})$ and $(k, \mu^{(2k)})$, for $\overline{pp}_{10.25}$ with truncation number $N = 64$. The dashed line (green) is $q_k^2 - q_k^4$, with x-axis the indices of Fourier modes $k = 1, 2, \cdots, N/2 - 1$. The inset is a magnification of the region containing the 8 leading entangled modes. As can be seen in table 1, for modes that follow, $k \geq 5$, the exponents are much smaller, in agreement with the expected separation into entangled and isolated modes of ref. [34]. For large indices, Floquet exponents appear in pairs corresponding to the real and imaginary part of Fourier modes. (d) The magnitudes of the Fourier components $|a_k| = |b_k + 1i * c_k|$ of the 1st, the 2nd, the 57th and 58th Floquet vectors $\mathbf{e}^{(k)}$ for $\overline{pp}_{10.25}$ at initial time $t = 0$, truncation number $N = 64$. For entangled modes the first 4 Fourier are comparable in magnitude. For the k_{th} isolated modes pair, the amplitude is concentrated on k_{th} Fourier mode. The x-axis is labeled by the Fourier mode indices. Only the $k > 0$ part is shown, the negative k follow by reflection.

Stability analysis of equilibria is crucial for understanding the the geometry of state space [21], but it is difficult for unstable periodic orbits due to lack of efficient and accurate numerical algorithms. Floquet theorem says that the Floquet matrix evaluated along a periodic orbit can be decomposed as a product of a periodic matrix and an exponential

Table 1: The first 10 and last four Floquet exponents and Floquet multiplier phases, $\Lambda_i = \exp(T\mu^{(i)} \pm i\theta_i)$, for orbits $\overline{pp}_{10.25}$ and $\overline{rp}_{16.31}$, respectively. θ_i column lists either the phase, if the Floquet multiplier is complex, or '-1' if the multiplier is real, but inverse hyperbolic. Truncation number $N = 64$. The 8 leading exponents correspond to the entangled modes: note the sharp drop in the value of the 9_{th} and subsequent exponents, corresponding to the isolated modes.

	$\overline{pp}_{10.25}$			$\overline{rp}_{16.31}$	
i	$\mu^{(i)}$	θ_i	i	$\mu^{(i)}$	θ_i
1,2	0.033209	±2.0079	1	0.32791	
3	-4.1096e-13		2	2.8679e-12	
4	-3.3524e-14	-1	3	2.3559e-13	
5	-0.21637		4	-0.13214	-1
6,7	-0.26524	±2.6205	5,6	-0.28597	±2.7724
8	-0.33073	-1	7	-0.32821	-1
9	-1.9605		8	-0.36241	
10	-1.9676	-1	9,10	-1.9617	±2.2411
...	...	...	...	...	...
59	-5313.6	-1	59	-5314.4	
60	-5317.6		60	-5317.7	
61	-6051.8	-1	61	-6059.2	
62	-6080.4		62	-6072.9	

matrix. We are interested in the eigenvalues (Floquet multipliers) and the corresponding eigenvectors (Floquet vectors) of the exponential matrix. More specifically, define a flow $x(t) = f^t(x(0))$ generated by velocity field $\dot{x} = v(x)$ with x a state vector. The evolution of perturbation along any orbit is governed by the Jacobian of this flow $J^t(x) = \partial f^t(x)/\partial x$, that is $\delta x(t) = J^t(x)\delta x(0)$, and Jacobian itself is evolved as follows,

$$\frac{dJ^t(x)}{dt} = A(x)J^t(x)\,, \quad A(x) = \frac{v(x)}{x}\,. \tag{5}$$

For a periodic orbit $x(T_p) = x(0)$, the solution of (5) for one period $J_p = J^T(x(0))$ is called Floquet matrix or monodromy matrix. $J_p e_i = e^{T(\mu^{(i)}+\omega^{(i)})}e_i$ gives the average expansion/contraction rate $\mu^{(i)}$ and invariant directions e_i in the tangent space.

For high dimensional nonlinear systems, Floquet exponents usually span a large number of orders, so one period integration of (5) usually results in a highly ill-conditioned Jacobian matrix, so we need to conduct transformations on each short-time Jacobian since whole matrix can be decomposed into the product of a sequence of square matrix. This is the basic idea of *Periodic Eigendecomposition*, and it is based on the idea on covariant vector algorithm and Periodic Schur Decomposition algorithm introduced in sec. 1.3. See [16] for the implementation details. Here, we only show the result with 1-dimensional Kuramoto-Sivashinsky equation defined on a periodic domain.

$$u_t + \frac{1}{2}(u^2)_x + u_{xx} + u_{xxxx} = 0\,,\ x \in [0, L] \tag{6}$$

Here domain size $L = 22$. Kuramoto-Sivashinsky equation is equivariant under reflection and space translation: $-u(-x,t)$ and $u(x+l,t)$ are also solutions if $u(x,t)$ is a solution. Based on the consideration of these symmetries, we focus on two types of orbits: preperiodic orbits $\hat{u}(0) = R\hat{u}(T_p)$ and relative periodic orbit, $\hat{u}(0) = g_p\hat{u}(T_p)$. Here R and g_p are reflection and rotation respectively.

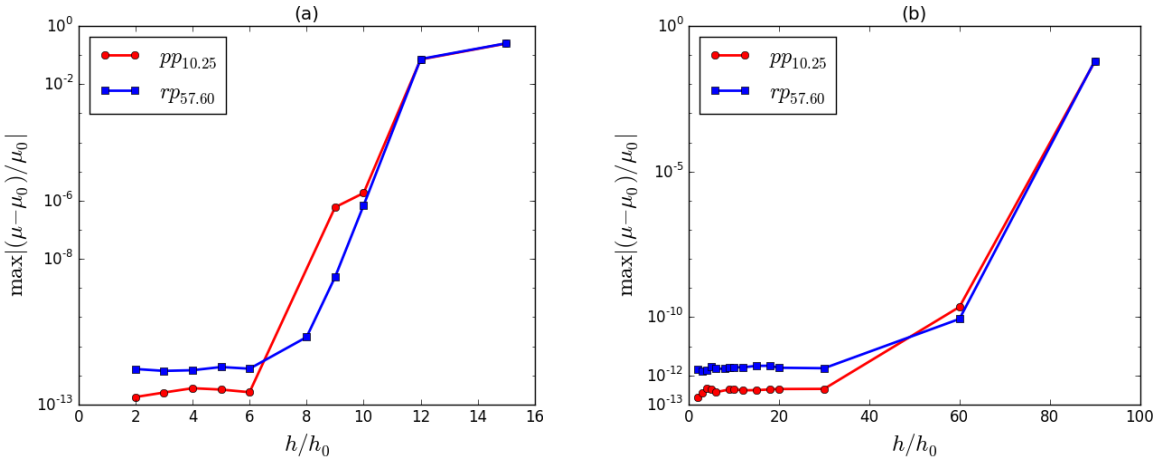

Figure 3: (Color online) Relative error of the real part of Floquet exponents associated with different time steps with which the Floquet matrix is integrated. Two orbits $\overline{pp}_{10.25}$ and $\overline{rp}_{57.60}$ are used as an example with the base case $h_0 \approx 0.001$. (a) The maximal relative difference of the whole set of Floquet exponents with increasing time step (decreasing the number of ingredient segments of the orbit). (b) Only consider the first 35 Floquet exponents.

At each repeat of the prime period, $\overline{pp}_{10.25}$ is invariant under reflection along $x = L/2$, figure 2 (a), and $\overline{rp}_{16.31}$ has a shift along the x direction as time goes on, figure 2 (b). Since $\overline{pp}_{10.25}$ and $\overline{rp}_{16.31}$ are both time invariant and equivariant under SO(2) group transformation $g(l)$, there should be two marginal Floquet exponents, corresponding to the velocity field and group tangent respectively. Table 1 shows that the 2_{nd} and 3_{rd}, respectively 3_{rd} and 4_{th} exponents of $\overline{rp}_{16.31}$, respectively $\overline{pp}_{10.25}$, are marginal, with accuracy as low as 10^{-12}, to which the inaccuracy introduced by the error in the closure of the orbit itself also contributes.

In practice, caution should be exercised when trying to determine the optimal number of time increments that the orbit should be divided into. Here we determined satisfactory m's by numerical experimentation shown in figure 3. Since larger time step means fewer time increments of the orbit, a very small time step ($h_0 \approx 0.001$) is chosen as the base case, and it is increased to test whether the corresponding Floquet exponents change substantially or not. As shown in figure 3 (a), up to $6h_0$ the whole Floquet spectrum varies within 10^{-12} for both $\overline{pp}_{10.25}$ and $\overline{rp}_{57.60}$. These two orbits represent two different types of invariant solutions which have short and long periods, so we presume that time step $6h_0$ is good enough for other short or long orbits too. On the other hand, if only the first few Floquet exponents are desired, the time step can be increased further to fulfill the job. As shown in figure 3 (b), if we are only interested in the first 35 Floquet exponents, then time step $30h_0$ is small enough. In high dimensional nonlinear systems, dynamics in the very contracting directions is, very the often, decoupled from the physical modes, and shed little insight into the system properties, so large time step could to used in order to save time. Table 1 and figure 2 (c) show that Periodic Schur Decomposition is capable of resolving Floquet multipliers differing by thousands of orders: when $N = 64$, the smallest Floquet multiplier for $\overline{pp}_{10.25}$ is $|\Lambda_{62}| \simeq e^{-6080.4\times 10.25}$.

The two marginal directions have a simple geometrical interpretation. Figure 4 (a) depicts the two marginal vectors of $\overline{pp}_{10.25}$ projected onto the subspace spanned by $[a_1, b_1, a_2]$

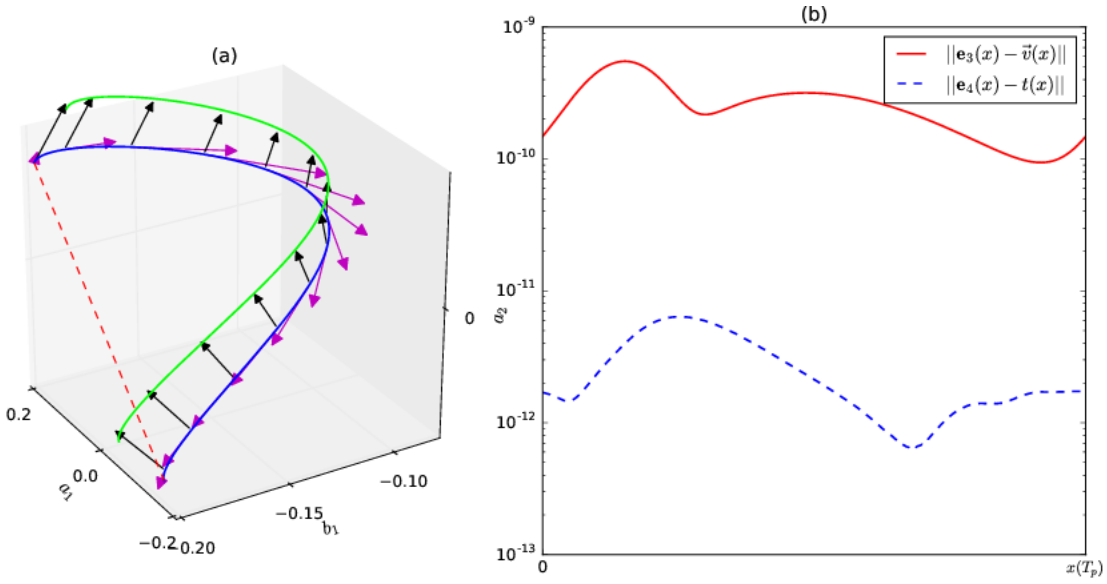

Figure 4: (Color online) Marginal vectors and the associated errors. (a) $\overline{pp}_{10.25}$ in one period projected onto $[a_1, b_1, a_2]$ subspace (blue curve), and its counterpart (green line) generated by a small group transformation $g(\ell)$, here arbitrarily set to $\ell = L/(20\pi)$. Magenta and black arrows represent the first and the second marginal Floquet vectors $\mathbf{e}^{(3)}(x)$ and $\mathbf{e}^{(4)}(x)$ along the prime orbit. (b) The solid red curve is the magnitude of the difference between $\mathbf{e}^{(3)}(x)$ and the velocity field $\vec{v}(x)$ along the orbit, and blue dashed curve is the difference between $\mathbf{e}^{(4)}(x)$ and the group tangent $t(x) = \mathbf{T}x$.

(the real, imaginary parts of the first mode and the real part of the second Fourier mode). The first marginal eigen-direction (the 3_{rd} Floquet vector in table 1) is aligned with the velocity field along the orbit, and the second marginal direction (the 4_{th} Floquet vector) is aligned with the group tangent. The numerical difference between the unit vectors along these two marginal directions and the corresponding physical directions is shown in figure 4 (b). The difference is under 10^{-9} and 10^{-11} for these two directions, which demonstrates the accuracy of the algorithm.

2.2 Local description of inertial manifold by Floquet vectors

Dissipative nonlinear systems described by partial differential equations are infinite dimensional in principle, but for a lot of them, there exists a finite dimensional inertial manifold and the dynamics is contained in it after a transient period of evolution. Here we try to explain the concept of "*slaving*" to understand how transition from infinite dimensional space into finite dimensional subspace happens. For strict mathematical treatment, see [29, 32]. Let u be a dynamical system in a finite or infinite dimensional Hilbert space H governed by

$$\frac{du}{dt} + Au + f(u) = 0 \tag{7}$$

Assume this system has a n-dimensional inertial manifold, and denote the projection from H to the first n eigenvectors of A by P. Let $Q = I - P$, then project (7) onto this subspace,

we obtain

$$\frac{dp}{dt} + Ap + Pf(p + \Phi(p)) = 0 \tag{8}$$

Here $p = Pu$ and $\Phi : PH \mapsto QH$. So we have reduced the dynamics to a subspace given the existence of such a mapping Φ, and the graph of Φ is the inertial manifold. Equation (8) is called the *inertial form* of this system. Essentially, the existence of inertial manifold indicates that the eigenmodes of A with index larger than n is slaved to its first n eigenmodes. For example, in Kuramoto-Sivashinsky equation, eigenmodes of A are Fourier modes, so short waves are slaved to long waves. Anyway, inertial manifold can be interpreted in different ways, but the essential idea is similar. See [25] for an adiabatic illustration by a simple two variable system.

To Approximate inertial manifold, or equivalently, to approximate mapping $\Phi : PH \mapsto QH$ requires the knowledge of its exact dimension. At present, people use empirical or some test number to truncate the original system. For example, in [18], 3 modes are used to represent the inertial manifold of 1-dimensional Kuramoto-Sivashinsky equation, but this truncated model is not enough to preserve the bifurcation diagram. On the other hand, mathematical upper bound for the dimension is not always tight. However, as stated in sec. 1.2, Recent progress in the numerical algorithm of covariant vectors enables us to expand tangent spaces into invariant subspaces. Covariant vectors computed along long ergodic trajectories are disentangled between the physical subspace and the transient subspace, which serves as a criteria for determining the effective dimension of the state space. This approach is different from the nonlinear Galerkin method since it has no ambition to use a static set of eigenvectors to describe the dynamics, it uses invariant vectors in the tangent space to linearly approximate the inertial manifold locally. From our intuition, we expect Floquet vectors along periodic orbits can give the same dimension of inertial manifold as covariant vectors. Moreover, Floquet vectors seem more suitable for this job. First, we have an efficient and accurate algorithm for calculating Floquet vectors introduced in sec 2.1, and do not need to follow an ergodic trajectory for a long time as covariant vector algorithm does. Second, periodic orbits are dense on the strange attractor and probably only a small subset of them is enough to represent the whole hierarchy in the system if the symbolic dynamics of this system is known, so experiments can be restricted to small number of short periodic orbits. But covariant vectors along ergodic trajectories reveals little information about the geometry of the strange attractor.

Angle distribution between physical and transient subspaces Like the experiments conducted in [31, 34], we measure the angle between subspaces spanned by disjoint Floquet vectors along periodic orbits inside the 1-dimensional Kuramoto-Sivashinsky equation with domain size $L = 22$. Since symbolic dynamics in this system is unknown, we choose to do the statics for all the periodic orbits available to us with period $T < 120$. As shown in figure 5, we are measuring the distribution of the angle between invariant subspace spanned by the first k Floquet vectors and the subspace spanned the remaining $30 - k$ Floquet vectors. Start from $k = 1$, As we add more into the first subspace, the possibility keeps nonzero until $k = 9$, and after which, the distribution shrinks away from zero. The same qualitative distribution is obtained for both pre-periodic orbits and relative periodic orbits. Therefore, the first 8 Floquet vectors are entangled with each other and are disentangled from the remaining set. We call the first set physical Floquet vectors and the latter unphysical one. The unphysical set has little effect on the dynamics in the neighborhood

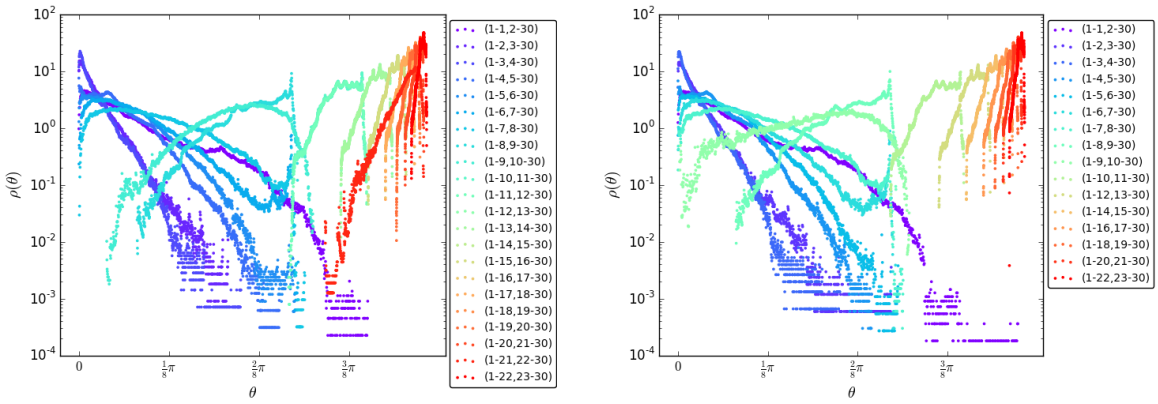

Figure 5: Angle distribution $\rho(\theta)$ versus θ for $\overline{ppo}$ (left) and $\overline{rpo}$ which has $T < 120$.

of this periodic orbit since all theses directions are contracting, and thus small perturbation inside it will die out eventually. So clearly, the first 8 Floquet vectors are enough to approximate the inertial manifold at the neighborhood of all the periodic orbits concerned in this experiment and we expect that such threshold number will not change if we can find more periodic orbits. Since periodic orbits are dense on the attractor, we expect the same number apply to the whole inertial manifold.

difference vectors spanned by subset of Floquet vectors Ergodic trajectories are attracted by periodic orbits along their stable directions, and repelled by their unstable directions. Each unstable direction is important since it determines how the system is stretched; however, if the inertial manifold exists, then only a subset of the stable directions have an effect on the dynamics asymptotically. So we believe that an ergodic trajectory is moving in a subspace which is spanned by the set of all unstable Floquet vectors and a subset of stable Floquet vectors around a periodic orbit locally. So, the number of Floquet vectors used to span such a subspace can be regarded as the dimension of inertial manifold.

We borrow the idea from [33] and conduct a set of experiments. We generate a long ergodic trajectory and try to find incidences that it shadows a specific periodic orbit. For each shadowing point x on the ergodic trajectory, we locate the nearest point x_p on the periodic orbit to it and defined the difference vector by $\Delta x = x - x_p$. When the orbit approaches or leaves the periodic orbit, the difference vector is mainly controlled by the stable and unstable Floquet vectors, so if we try to expand Δx using a subset of Floquet vectors and see how many of Floquet vectors is enough for a faithful expansion, we could almost get a faithful approximation of the inertial manifold locally. In figure 6, if more than 7 Floquet vectors are used, then the tendency shows that θ will diminish to zero linearly as Δx goes to zero, which is not true if no more than 6 Floquet vectors are used to span the subspace. Note the experiments are conducted in the symmetry-reduced state space, so the dimension of inertial manifold of the full state space is $7 + 1$, which is consistent with the previous result.

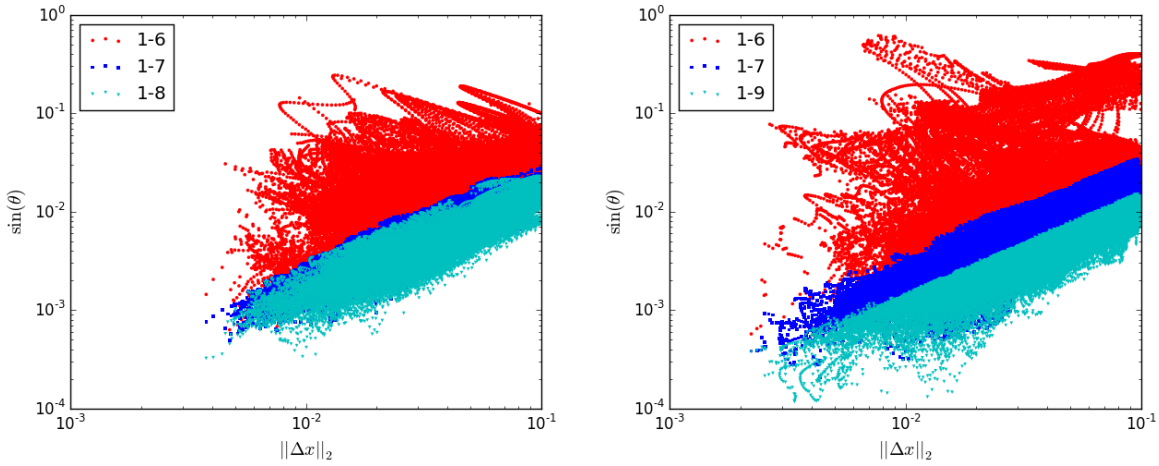

Figure 6: scatter plot of $sin\theta$ vs the norm of difference vector. θ is the angle between Δx and the subspace spanned by a subset of Floquet vectors. (a) $\overline{ppo}_{32.36}$ with 198 shadowing incidences. (b) $\overline{rpo}_{34.64}$ with 230 shadowing incidences.

index	λ
1,2	0.1474653 ± 17.2375582i
3,4	0.1474643 ± 17.2375572i
5	-7.21620620e-14
6	-1.86242571e-13
7,8	-0.1002241 ± 17.6645298i
9,10	-0.1008975 ± 17.6556189i

Table 2: The first 10 stability exponents of relative equilibrium figure 8.

2.3 Traveling wave in cubic quintic complex Ginzburg-Landau equation

In cubic quintic complex Ginzburg-Landau (4), traveling wave (relative equilibrium) is defined as a solution of

$$A(x,0) = e^{i\phi}A(x+ct,t)$$

which is

$$a_k(0) = e^{i\omega_\rho t}e^{ik\omega_\tau t}a_k(t) \tag{9}$$

in Fourier space. Here ω_ρ is the velocity in the group tangent of phase invariance symmetry: $\phi = \omega_\rho t$, and $\omega_\tau = 2\pi/L \cdot c$. Levenberg-Marquardt algorithm is implemented to solve (9) with random initial conditions. Dozens of relative equilibria are founded and a few are shown in figure 7. Some of them are extensive spanning the whole domain; others are localized. Here I are only interested in the one related to the soliton (1) shown in figure 8. This relative equilibrium has group velocity $\omega_\tau = 0$ and $\omega_\rho = 17.6675$. Figure 8 shows the profile of this relative equilibrium and its stability exponents. Table 2 gives the numerical values of these exponents.

There are two marginal directions, which correspond to the group tangents of translational symmetry and phase invariance. Note the velocity field lies in this two dimensional subspace. Four unstable directions are in two conjugate pairs, with almost the same expan-

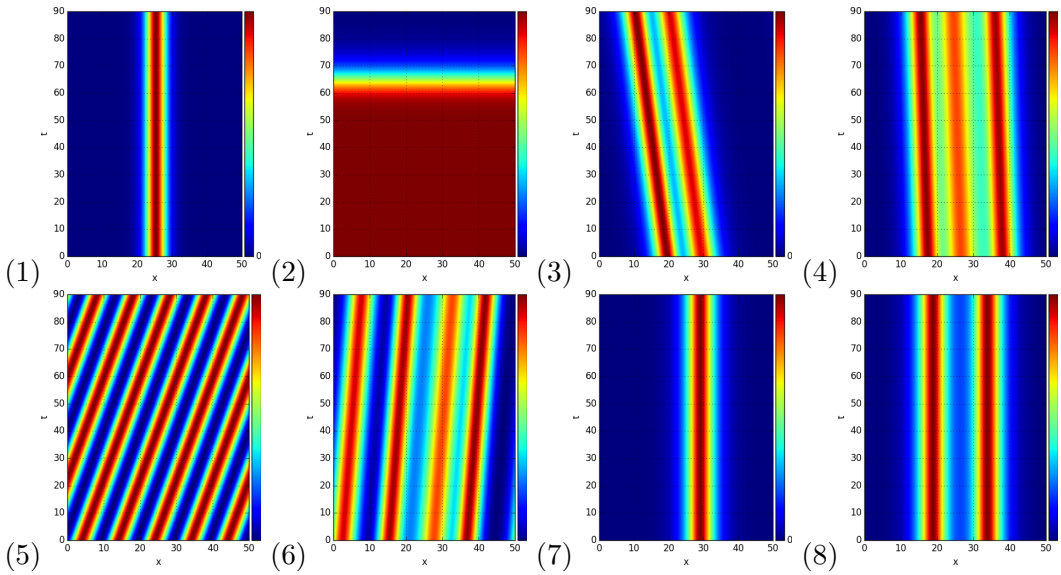

Figure 7: A set of different relative equilibria. (1) is different from (7) by the phase velocity. Plane wave solutions like (2) appear most frequently, and there is a set of solutions like (2) with different phase velocities and translational velocities. Only one representative is shown here.

sion rates. The corresponding eigenvectors have almost the same profile. [1] Also, the profile is slightly asymmetric as shown in figure 9(a)(b). On the other hand, since this system has reflection symmetry. The real/imaginary part of the leading eigenvector of the reflected state is shown in figure 9(c)(d). The left side is larger than the right side for this reflected state. Note that the unstable directions have should profile and the peaks are exactly at the place where explosion happens. In this sense, explosions are just homoclinic connections of this relative equilibrium.

Actually, ref. [1] uses an approximation method to approximate the unstable directions, and gets a symmetric and an asymmetric solutions, which are used to explain the symmetric and asymmetric explosions. Here we only got 4 slightly asymmetric solutions, but they have reflection symmetry, which means that if there are perturbations at both sides of the soliton, then symmetric explosion also could occur. Also this is a pure numerical result. No approximation is used.

Next, I will investigate the unstable manifold of this relative equilibrium to see how the flow is organized around this relative equilibrium. But before that, we need to reduce all the symmetries mentioned in sec. 1.4 and then work on the symmetry-reduced state space.

Reduce continuous symmetries The two continuous symmetry operations in cubic quintic complex Ginzburg-Landau system can be regarded as one Lie group of two generators, since these two symmetries commute. $g(\theta, \phi) = g_\tau(\theta) g_\rho(\phi)$ produces translation in Fourier space as

$$a_k(t) \to a_k(t) e^{i(k\theta+\phi)} \tag{10}$$

[1] Predrag: 2015-09-06 We had explained in the blog why exponents come in 'almost' quadruplets. Is it worth including that here? In any case, that must go into the thesis.

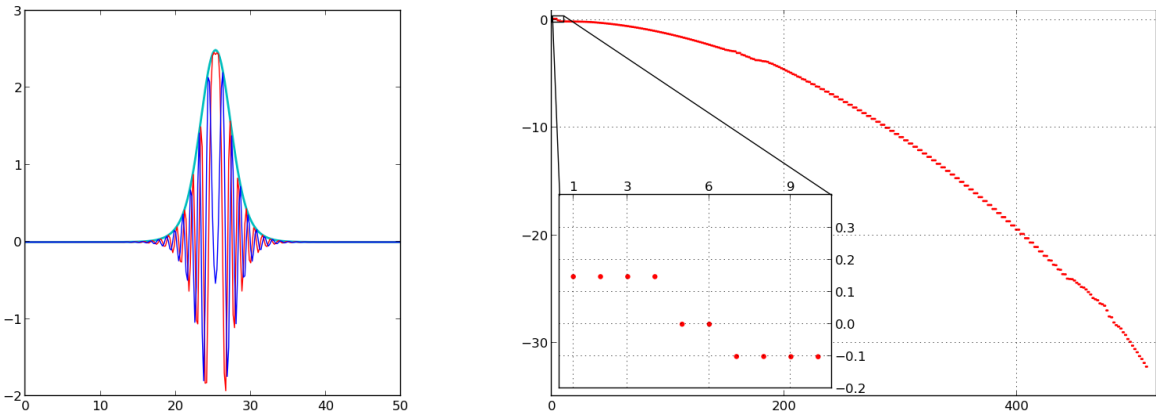

Figure 8: (Left panel) Spatial profile of the relative equilibrium (1) at some instant, and the real parts of the spectrum of stability exponents of this relative equilibrium. The green line is the magnitude of the relative equilibrium. Red and blue lines are respectively its real and imaginary parts. (Right panel) Stability spectrum.

In order to reduce this continuous symmetry, we define a subspace on which all points has vanishing imaginary part of the 1st and -1st modes

$$Im(a_1) = Im(a_{-1}) = 0\,,$$

and transform all points in the full state space to this subspace by $x(\tau) = g(\theta_s, \phi_s)\,\hat{x}(\tau)$ with

$$\phi_s = \frac{1}{2}(\alpha_1 + \alpha_{-1})\,, \quad \theta_s = \frac{1}{2}(\alpha_1 - \alpha_{-1})\,. \tag{11}$$

Here, $\alpha_{\pm 1}$ are the phase angle of ± 1 mode. Subscript s denotes the specific angle from slice to full state space.

On the other hand, this choice of slice introduces phase wrapping problem. From (11), when α_1 or α_{-1} is wrapped, namely, jumps 2π suddenly, ϕ_s and θ_s jumps π. Therefore, at this point, trajectory in the slice is not continuous. More importantly, it also means that we have introduced another discrete symmetry. Each orbit in the full state space has 2 corresponding orbits in the slice, which are related by $g(\pi, \pi)$. You can have a feeling of how well slice works in figure 10

Reduce reflection symmetry To illustrate the procedure of reducing reflection symmetry, we'd better split the real and imaginary part the Fourier modes $a_k = b_k + 1i * c_k$ and work on the state space defined by

$$[b_0, c_0, b_1, c_1, \cdots, b_{N/2-1}, c_{N/2-1}, b_{-N/2+1}, c_{-N/2+1}, \cdots, b_{-1}, c_{-1}]\,, \tag{12}$$

Reflection symmetry ($a_k \to a_{-k}$) in state space (12) is

$$(b_0, c_0, b_1, c_1, b_2, c_2, \cdots, b_{-1}, c_{-1}) \Rightarrow (b_0, c_0, b_{-1}, c_{-1}, b_{-2}, c_{-2}, \cdots, b_1, c_1) \tag{13}$$

Our strategy is reducing continuous symmetries first, then reducing reflection symmetry. Inspecting (13), you find that a state point in slice under reflection is still in the slice. You can analogize it to the case in a 3-d space: we choose a 2-d plane slice which is perpendicular

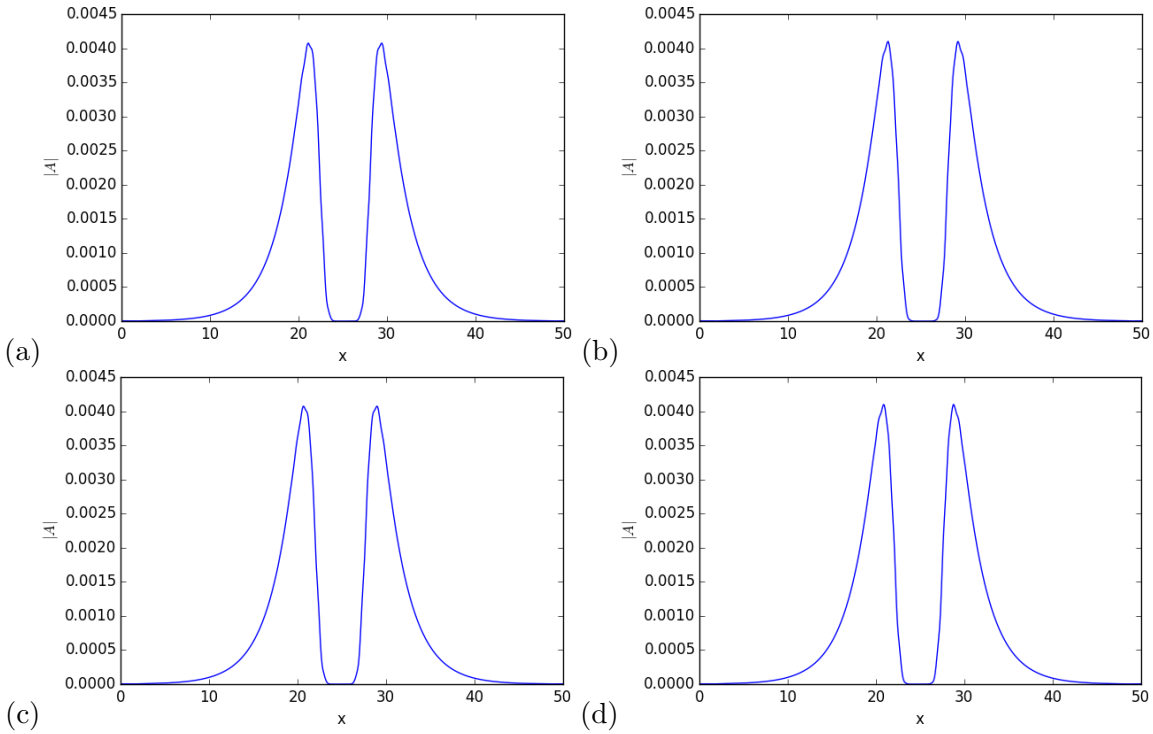

Figure 9: Eigenvectors of the relative equilibrium. (a)(b) the magnitude of the real/imaginary part of the 1st eigenvector of the relative equilibrium. (c)(d) The relative equilibrium is reflected $A(x) \to A(-x)$. The magnitude of the real/imaginary part of the 1st eigenvector of the reflected relative equilibrium.

to the reflection axis. Therefore, a point in slice will be reflected to another point in the slice by the original reflection operation. This is the exact reason for the choice of this specific slice.

Now we try to reduce symmetry (13). We take a 3-step approach. First perform a linear transformation

$$\begin{aligned}&(b_0, c_0, b_1, c_1, b_2, c_2, \cdots, b_{-1}, c_{-1}) \Rightarrow \\ &(b_0, c_0, \frac{b_1 - b_{-1}}{2}, \frac{c_1 - c_{-1}}{2}, \frac{b_2 - b_{-2}}{2}, \frac{c_2 - c_{-2}}{2}, \cdots, \frac{b_1 + b_{-1}}{2}, \frac{c_1 + c_{-1}}{2})\end{aligned} \tag{14}$$

Denote the transformed state as $(b_0, c_0, p_1, q_1, \cdots, q_{N/2-1}, p_{-N/2+1}, \cdots, p_{-1}, q_{-1})$. So under reflection, $p_i\,, q_i$ with $i < 0$ keep unchanged, but $p_i\,, q_i$ with $i > 0$ flip sign. In the second stage, we perform a nonlinear transformation:

$$\begin{aligned}&(b_0, c_0, p_1, q_1, p_2, q_2, \cdots, q_{N/2-1}, p_{-N/2+1}, \cdots, p_{-1}, q_{-1}) \Rightarrow \\ &(b_0, c_0, r_1, s_1, r_2, s_2, \cdots, s_{N/2-1}, p_{-N/2+1}, \cdots, p_{-1}, q_{-1})\end{aligned} \tag{15}$$

Here $p_i\,, q_i$ with $i < 0$ are unchanged.

$$r_1 = \frac{p_1^2 - q_1^2}{\sqrt{p_1^2 + q_1^2}}\,, s_1 = \frac{p_1 q_1}{\sqrt{p_1^2 + q_1^2}}\,, r_2 = \frac{q_1 p_2}{\sqrt{q_1^2 + p_2^2}}\,, s_2 = \frac{p_2 q_2}{\sqrt{p_2^2 + q_2^2}}\,, \cdots$$

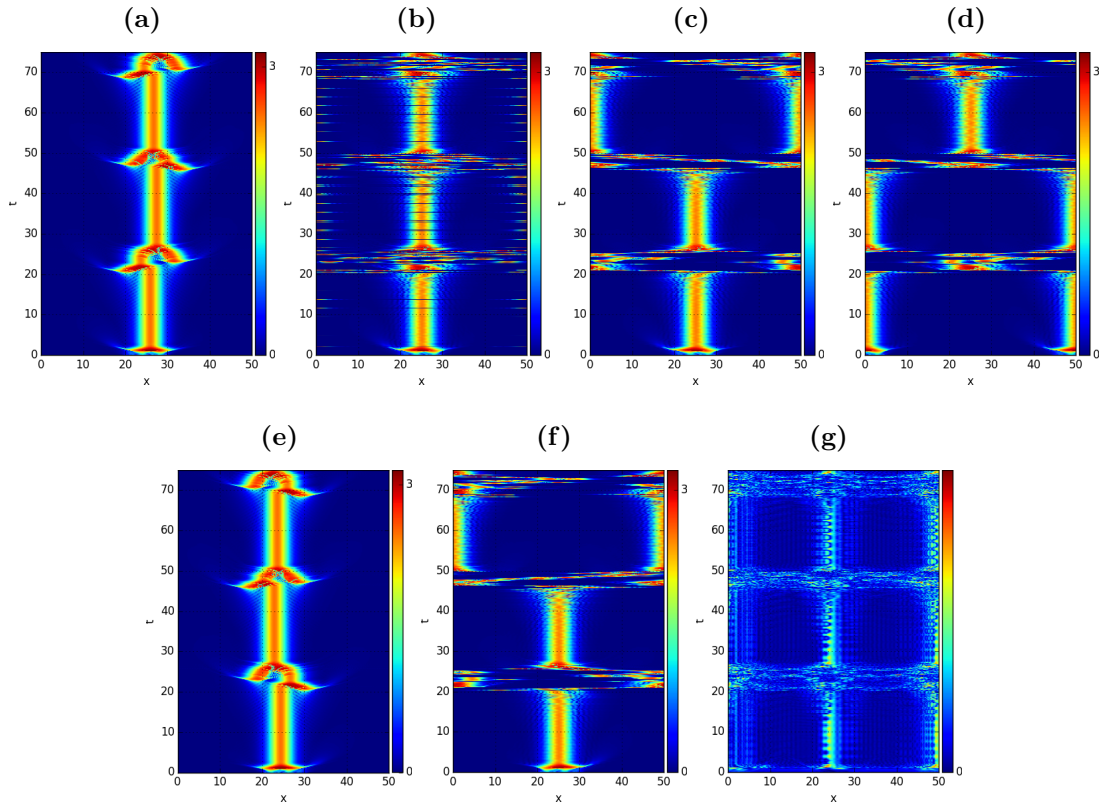

Figure 10: (a) Full state space trajectory. (b) Continuous symmetry reduced of (a) with wrapped phase. (c) Continuous symmetry reduced of (a) with unwrapped phase. (d) rotated by $g(\pi, \pi)$ of (c). (e) The reflected states of (a). (f) Continuous symmetry reduced of (e). (g) after reducing all symmetries of (a)(b).

The previous two steps reduce the reflection symmetry of original system $a_k \to a_{-k}$; however, the specific choice of slice introduces another reflection symmetry: even modes flip sign.

$$(b_0, c_0, b_1, c_1, b_2, c_2, \cdots, b_{-1}, c_{-1}) \Rightarrow (-b_0, -c_0, b_{-1}, c_{-1}, -b_{-2}, -c_{-2}, \cdots, b_1, c_1) \tag{16}$$

Under representation (15), this reflection turns to be

$$(b_0, c_0, r_1, s_1, r_2, s_2, \cdots, s_{N/2-1}, p_{-N/2+1}, \cdots, p_{-1}, q_{-1}) \Rightarrow$$
$$(-b_0, -c_0, r_1, s_1, -r_2, s_2, \cdots, -r_{N/2-1}, s_{N/2-1}, p_{-N/2+1}, q_{-N/2+1}, -p_{-N/2+2}, -q_{-N/2+2}, \cdots, p_{-1}, q_{-1})$$

Terms $(b_0, c_0, r_2, \cdots, r_{N/2-1}, p_{-N/2+2}, q_{-N/2+2}, \cdots, p_{-2}, q_{-2})$ flip sign, so we can utilize the same formulation to reduce this reflection symmetry:

$$(b_0, c_0, r_2, \cdots, r_{N/2-1}, p_{-N/2+2}, q_{-N/2+2}, \cdots, p_{-2}, q_{-2}) \Rightarrow (t_1, t_2, \cdots, t_{N-2}) \tag{17}$$

$$t_1 = \frac{b_0^2 - c_0^2}{\sqrt{b_0^2 + c_0^2}}, t_2 = \frac{b_0 c_0}{\sqrt{b_0^2 + c_0^2}}, t_3 = \frac{r_2 c_0}{\sqrt{r_2^2 + c_0^2}}, t_3 = \frac{r_3 r_2}{\sqrt{r_3^2 + r_2^2}}, \cdots$$

In conclusion, the following coordinate reduces all symmetries inside this system.

$$(t_1, t_2, r_1, s_1, t_3, s_2, \cdots, s_{N/2-1}, p_{-N/2+1}, \cdots, p_{-1}, q_{-1})\,. \tag{18}$$

Figure 10 (g) shows the state after reducing all symmetries of this system. When only continuous symmetry is reduced, (a),(e) become (c) and (f) respectively. Note, (f) is exactly a reflection image of (c). If Reflection symmetries are reduced further, (c) (d) (f) all turn to (g).

3 Plan for future work

3.1 Dimension of inertial manifold

We have only tested the method described in sec. 2.2 to investigated the dimension of inertial manifold in 1-dimensional Kuramoto-Sivashinsky equation, but we think this method can be applied to other turbulent systems as well, for example complex Ginzburg-Landau equation, 2-d or 3-d Navier-Stokes equation. The point we conduct such research to other systems in the next step is that usually the mathematical proof of existence of inertial manifold sheds limited information about its exact dimension. Moreover, for systems like 3-d Navier-Stokes, the existence of inertial manifold is still unknown, so the experiments investigating decoupling in the tangent space by Floquet vectors can serve as a valuable tool to provide accurate enough information about the local geometry of inertial manifold ahead of strict mathematical statements. Also, this information can help engineers to use the appropriate resolution in the numerical turbulence simulation.

3.2 Cycle expansions for cubic quintic complex Ginzburg-Landau equation

We have found quite a few relative equilibriums in 1-d cubic quintic complex Ginzburg-Landau equation and converted the dynamics into the symmetry-reduced space. The next step is trying to find periodic orbits or relative periodic orbits inside this system and hopefully build the symbolic dynamics according to the geometry of this hierarchy of periodic orbits.

with this set of periodic orbits, cycle expansion can be applied to spectral determinant (1) with interesting physical quantity such as diffusion rate as the observable. Therefore, our ultimate goal of studying cubic quintic complex Ginzburg-Landau equation is to give exact prediction about the long time behavior of soliton solution in it. Also such method can be applied to the 2-d cubic quintic complex Ginzburg-Landauand analyze the diffusion constant of the random walk reported in [7].

References

[1] N. Akhmediev and J. M. Soto-Crespo. Strongly asymmetric soliton explosions. *Phys. Rev. E*, 70, 2004.

[2] R. Artuso, E. Aurell, and P. Cvitanović. Recycling of strange sets: I. Cycle expansions. *Nonlinearity*, 3:325–359, 1990.

[3] R. Artuso, E. Aurell, and P. Cvitanović. Recycling of strange sets: II. Applications. *Nonlinearity*, 3:361–386, 1990.

[4] R. Artuso, H. H. Rugh, and P. Cvitanović. Why does it work? In *Chaos: Classical and Quantum*. Niels Bohr Inst., Copenhagen, 2016.

[5] A. Bojanczyk, G. H. Golub, and P. Van Dooren. The periodic Schur decomposition. Algorithms and applications. In *Proc. SPIE Conference*, pages 31–42, 1992.

[6] N. B. Budanur, D. Borrero-Echeverry, and P. Cvitanović. Periodic orbit analysis of a system with continuous symmetry - A tutorial. *Chaos*, 25:073112, 2015.

[7] C. Cartes, J. Cisternas, O. Descalzi, and H. R. Brand. Model of a two-dimensional extended chaotic system: Evidence of diffusing dissipative solitons. *Phys. Rev. Lett.*, 109:178303, 2012.

[8] F. Christiansen, P. Cvitanović, and V. Putkaradze. Spatiotemporal chaos in terms of unstable recurrent patterns. *Nonlinearity*, 10:55–70, 1997.

[9] J. Cisternas and O. Descalzi. Intermittent explosions of dissipative solitons and noise-induced crisis. *Phys. Rev. E*, 88:022903, 2013.

[10] J. Cisternas, O. Descalzi, and C. Cartes. The transition to explosive solitons and the destruction of invariant tori. *Cent. Eur. J. Phys.*, 10:660–668, 2012.

[11] M. C. Cross and P. C. Hohenberg. Pattern formation outside of equilibrium. *Rev. Mod. Phys.*, 65:851–1112, 1993.

[12] P. Cvitanović, R. Artuso, R. Mainieri, G. Tanner, and G. Vattay. *Chaos: Classical and Quantum*. Niels Bohr Inst., Copenhagen, 2016.

[13] R. J. Deissler and H. R. Brand. Periodic, quasiperiodic, and chaotic localized solutions of the quintic complex Ginzburg-Landau equation. *Phys. Rev. Lett.*, 72:478–481, 1994.

[14] O. Descalzi and H. R. Brand. Transition from modulated to exploding dissipative solitons: Hysteresis, dynamics, and analytic aspects. *Phys. Rev. E*, 82:026203, 2010.

[15] O. Descalzi, C. Cartes, J. E. Cisternas, and H. R. Brand. Exploding dissipative solitons: The analog of the Ruelle-Takens route for spatially localized solutions. *Phys. Rev. E*, 83:056214, 2011.

[16] X. Ding and P. Cvitanović. Periodic eigendecomposition and its application in Kuramoto-Sivashinsky system. *SIAM J. Appl. Dyn. Syst.*, 15:1434–1454, 2016.

[17] J.-P. Eckmann and D. Ruelle. Ergodic theory of chaos and strange attractors. *Rev. Mod. Phys.*, 57:617–656, 1985.

[18] C. Foias, M. S. Jolly, I. G. Kevrekidis, G. R. Sell, and E. S. Titi. On the computation of inertial manifolds. *Phys. Lett. A*, 131:433–436, 1988.

[19] C. Foias, G. R. Sell, and R. Temam. Inertial manifolds for nonlinear evolutionary equations. *J. Diff. Equ.*, 73:309–353, 1988.

[20] F. Ginelli, H. Chaté, R. Livi, and A. Politi. Covariant Lyapunov vectors. *J. Phys. A*, 46:254005, 2013.

[21] J. Guckenheimer and P. Holmes. *Nonlinear Oscillations, Dynamical Systems, and Bifurcations of Vector Fields*. Springer, New York, 1983.

[22] M. Jolly, R. Rosa, and R. Temam. Evaluating the dimension of an inertial manifold for the Kuramoto-Sivashinsky equation. *Advances in Differential Equations*, 5:31–66, 2000.

[23] P. V. Kuptsov and U. Parlitz. Theory and computation of covariant Lyapunov vectors. *J. Nonlinear Sci.*, 22:727–762, 2012.

[24] Y. Lan and P. Cvitanović. Unstable recurrent patterns in Kuramoto-Sivashinsky dynamics. *Phys. Rev. E*, 78:026208, 2008.

[25] P. Manneville. *Dissipative Structures and Weak Turbulence*. Academic, New York, 1990.

[26] M. Marion and R. Temam. Nonlinear Galerkin methods. *SIAM J. Numer. Anal.*, 26:1139–1157, 1989.

[27] V. I. Oseledec. A multiplicative ergodic theorem. Liapunov characteristic numbers for dynamical systems. *Trans. Moscow Math. Soc.*, 19:197–221, 1968.

[28] J. C. Robinson. Inertial manifolds for the Kuramoto-Sivashinsky equation. *Phys. Lett. A*, 184:190–193, 1994.

[29] J. C. Robinson. Finite-dimensional behavior in dissipative partial differential equations. *Chaos*, 5:330–345, 1995.

[30] D. Ruelle. Ergodic theory of differentiable dynamical systems. *Publ. Math. IHES*, 50:27–58, 1979.

[31] K. A. Takeuchi, H. L. Yang, F. Ginelli, G. Radons, and H. Chaté. Hyperbolic decoupling of tangent space and effective dimension of dissipative systems. *Phys. Rev. E*, 84:046214, 2011.

[32] R. Temam. *Infinite-Dimensional Dynamical Systems in Mechanics and Physics*. Springer, New York, 2 edition, 2013.

[33] H. L. Yang and G. Radons. Geometry of inertial manifold probed via Lyapunov projection method. *Phys. Rev. Lett.*, 108:154101, 2012.

[34] H. L. Yang, K. A. Takeuchi, F. Ginelli, H. Chaté, and G. Radons. Hyperbolicity and the effective dimension of spatially extended dissipative systems. *Phys. Rev. Lett.*, 102:074102, 2009.